Ab Initio Simulations of Tritium Diffusion in Al$_2$O and Intermetallic Al$_{12}$(TM)$_{2.34}$ Aluminide Coating Phases

September 2023

Michel Sassi
David J. Senor
Andrew M. Casella

DISCLAIMER

Ab Initio Simulations of Tritium Diffusion in Al$_2$O and Intermetallic Al$_{12}$(TM)$_{2.34}$ Aluminide Coating Phases

September 2023

Michel Sassi
David J. Senor
Andrew M. Casella

Summary

Density functional theory simulations have been carried out to investigate the diffusion of interstitial tritium in $Al_{12}(TM)_{2.34}$ and Al_2O bulk phases. In $Al_{12}(TM)_{2.34}$ the transition metal (TM) sites are occupied on average by 58.93 at.% Fe, 18.52 at.% Cr, and 22.54 at.% Ni. While the insertion of interstitial tritium in Al_2O lead to a strong disordering of the structure, we only investigated interstitial tritium in $Al_{12}(TM)_{2.34}$ and its iron end-member (i.e., $Al_{12}Fe_{2.34}$). Nine diffusion pathways have been investigated along the *a*-, *b*-, and *c*-axis of $Al_{12}(TM)_{2.34}$. The direction of fastest diffusion for interstitial tritium is found to be along the *b*-axis, with a calculated diffusion coefficient of $\approx 10^{-10}$ $m^2.s^{-1}$ at 600 K, which is at least one order of magnitude faster than those previously calculated for interstitial tritium in other Al-rich phases such as Fe_2Al_x, Fe_4Al_{13}, and $FeNiAl_5$ for which $D_T \leq 10^{-11}$ $m^2.s^{-1}$, $\approx 10^{-12}$ $m^2.s^{-1}$, and $D_T \approx 10^{-13}$ $m^2.s^{-1}$ respectively. The comparison of the energy landscape between $Al_{12}(TM)_{2.34}$ and $Al_{12}Fe_{2.34}$ for the fastest diffusion pathways in each axis direction, found that some pathways are not sensitive to transition metal mixing, while other are more affected, leading to higher energy barrier in $Al_{12}Fe_{2.34}$ in part due to a more energetically favorable formation of Fe—T bond compared to Ni—T. However, we found that both materials have similar diffusion coefficients as the fastest diffusion pathways occurs along pathways that are not very sensitive to transition metal mixing.

1.0 Introduction

Reports[1,2] have indicated that a small but steady fraction of atomic tritium generated in ^{6}Li enriched γ-LiAlO$_2$ pellets during neutron irradiation permeates out of the TPBAR during production. While attempts to mitigate tritium release in the coolant by modifying the design of the TPBAR were ineffective,[1] it has been recognized that efforts should be devoted to developing an understanding of the irradiation behavior of the various TPBAR components and a mechanistic understanding of tritium transport within the TPBAR during irradiation. Ultimately, it is expected that with a better knowledge of tritium transport and interactions within the pellets, getters, coating, and cladding components of the TPBAR, performance models will provide much more reliable tritium distribution predictions.

In the design of the TPBAR[3] an aluminide coating, essentially made of Fe-Al phases, is in contact with an inner helium filled gas plenum and a 316 stainless steel (316 SS) cladding. In 2020, Jiang *et al.*[4] have conducted STEM imaging combined with energy-dispersive X-ray spectroscopy (EDS) of neutron irradiated coating samples and found that an aluminum oxide layer (Al$_2$O$_3$) of 50 nm thick was formed at the surface of the aluminide coating. In 2022, M. Olszta[5] performed STEM-EDS mapping of unirradiated archived coating samples and also found that an aluminum oxide (Al$_2$O$_3$) layer was formed at the surface of the aluminide coating. Further STEM investigations revealed that below the oxidized surface, a large near surface region of about 10 μm thick was contaminated with Cr, Ni, and Fe. The combination of atomic column imaging and associated diffraction analysis indicated that this near surface region is crystalline and that an intermetallic orthorhombic Al-phase containing transition metals (TM) at an approximate composition of Al$_{12}$(TM)$_{2.34}$ is present in a large portion of the 10 μm near surface region. While complete TEM composition identification is challenging due to the chemical complexity of the coating samples, STEM-EDS and SEM chemical analysis revealed that the TM sites are on average 58.93 at.% Fe, 18.52 at.% Cr, and 22.54 at.% Ni. It was further revealed that the transition between surface Al$_2$O$_3$ and near surface intermetallic Al$_{12}$(TM)$_{2.34}$ involves cubic Al$_2$O.

To provide a mechanistic understanding of tritium transport within TPBAR's aluminide coating, we performed *ab initio* simulations of interstitial tritium diffusion in bulk Al$_{12}$(TM)$_{2.34}$ phase recently observed by STEM in the near surface region. While it was initially planned to investigate tritium diffusion in the Al$_2$O phase, we found that this bulk material is highly unstable to the insertion of tritium species, leading to highly disordered phase. With such change in the structure, the investigation of tritium diffusion in Al$_2$O has not been conducted as it is not relevant to the actual structure observed experimentally. Nevertheless, the findings obtained for tritium diffusion in bulk Al$_{12}$(TM)$_{2.34}$ will be compared to previous studies of interstitial tritium diffusion in other major Al-rich phases also found in the aluminide coating[6] and provide a more complete picture of tritium transport in complex chemical environments.

2.0   Computational Details

Density functional theory calculations have been performed with the VASP code.[7] All the simulations used the generalized gradient approximation (GGA) exchange-correlation as parametrized in the Perdew, Burke, and Ernzerhof (PBE) functional.[8] A cutoff energy of 350 eV for the plane-wave basis set has been used and spin-polarization has been taken into account. Prior to introducing interstitial tritium in either $Al_{12}(TM)_{2.34}$[9] or Al_2O,[10] the lattice parameters and atomic coordinates of defect-free bulk phases were fully relaxed using a convergence criterion of 10^{-5} eV/cell for the total energy and 10^{-4} eV/Å for the force components. As shown in Table 1, for $Al_{12}(TM)_{2.34}$ and Al_2O, the Brillouin zone has been respectively sampled with a Monkhorst-Pack[11] k-point mesh of 3×3×2 and a Γ-centered mesh of 5×5×5. After the addition of interstitial tritium, only the atomic coordinates were allowed to relax, while the lattice parameters were kept fixed to their relaxed defect-free bulk structures values. Due to their similar electronic structure, the pseudopotential of standard hydrogen (^1H) has been used to describe tritium (^3H), however, to account for the isotopic effect, the mass in the pseudopotential has been modified to matches that of the isotope atom. Several diffusion pathways have been investigated and the energy barrier has been determined by using the climbing image nudged elastic band method[12,13] (CI-NEB). In this study, we focused on neutral interstitial tritium atoms.

| Phase	Supercell size	k-point mesh
$Al_{12}(TM)_{2.34}$	1×1×1 (306 atoms)	3×3×2
Al_2O	2×2×2 (96 atoms)	5×5×5

Table 1: Summary of the supercell sizes and k-point mesh sampling used in this study.

3.0 Results and Discussion

## 3.1 Crystal structure of $Al_{12}(TM)_{2.34}$ and Al_2O

Before investigating the diffusion of interstitial tritium in $Al_{12}(TM)_{2.34}$, a satisfactory periodic model structure for the orthorhombic $Al_{12}(TM)_{2.34}$ bulk phase, which contains 306 atoms (~21 formula units), needs to be determined. As shown in Figure 1a, the experimentally available structure of $Al_{12}(TM)_{2.34}$[9] has two major unknowns: (*i*) the distribution of the Fe, Cr, and Ni species is not known as only the position of a "transition metal" (TM) is provided. (*ii*) The Al atoms surrounding some of the TM sites, highlighted by blue polyhedron and yellow spheres, have a partial occupancy which makes a periodic atomic model hard to build and give rise to a total of 8064 possible structural combinations. To resolve these challenges, we used a structure generation approach[14] to calculate the energy of more than 1000 symmetrically inequivalent structures to determine the preferred positions of the Al sites with partial occupancies for the specific case where all TM sites are occupied by Fe species (i.e., $Al_{12}Fe_{2.34}$). Once the preferred position of Al species around some TM sites were found, we explored various Fe, Cr, and Ni combinations for the transition metal sites, keeping in mind that the ideal Fe:Cr:Ni fraction should be close to the experimental averages of 58.93 at.% Fe, 18.52 at.% Cr, and 22.54 at.% Ni. As the number of transition metal sites in the unit cell is 50, the optimal Fe:Cr:Ni ratio has been fixed to 30 Fe atoms, 9 Cr atoms, and 11 Ni atoms. The final $Al_{12}(TM)_{2.34}$ structure used for the simulations is shown in Figure 2a. The optimized lattice parameters for $Al_{12}Fe_{2.34}$ were a=12.341 Å (+0.01%), b=12.443 Å (+0.27%), and c=29.980 Å (-2.38%), and those of $Al_{12}(TM)_{2.34}$ were a=12.406 Å (+0.53%), b=12.465 Å (+0.44%), and c=30.140 Å (-1.85%), which are in good agreement with the experimental lattice parameters of a=12.340 Å, b=12.410 Å, and c=30.710 Å.[9]
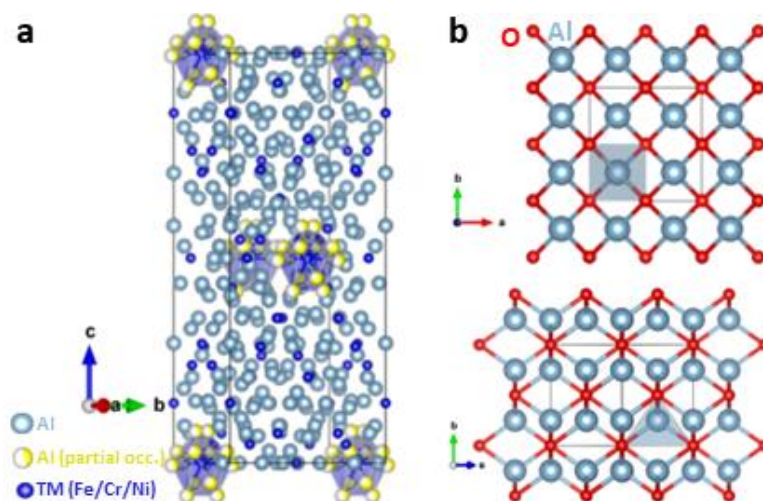
Figure 1: Visual representation of (a) bulk $Al_{12}(TM)_{2.34}$ and (b) bulk cubic Al_2O.

The Al$_2$O bulk phase considered in this work for tritium diffusion is cubic, as shown in Figure 1b, and has been observed by TEM[5] sandwiched between the surface Al$_2$O$_3$ and near surface intermetallic Al$_{12}$(TM)$_{2.34}$ phases. In Al$_2$O, each Al atom is located in a tetrahedral site, as shown by the polyhedral representation in Figure 1b. The optimization of a 2×2×2 supercell leads to a lattice parameter a=5.692 Å (+14.31%), which is greatly overestimated compared to the experimental value of 4.980 Å.[10] In the experimental cubic structure, all Al—O bond lengths are 2.156 Å, while they are 2.465 Å in the optimized structure. While the optimized defect-free Al$_2$O structure remains cubic, the fact that such large structural discrepancies are obtained between experimental and calculated lattice parameters and bond lengths suggest that this material phase could be unstable at the conditions of DFT simulations (i.e., 0 K temperature). The instability of lower oxide of aluminum at room temperature has been highlighted by Hoch *et al.*[10] during the making of high temperature AlO (1700°C) and Al$_2$O (1100°C) solid phases. We will discuss later the effects of tritium introduction in the lattice at a later stage.
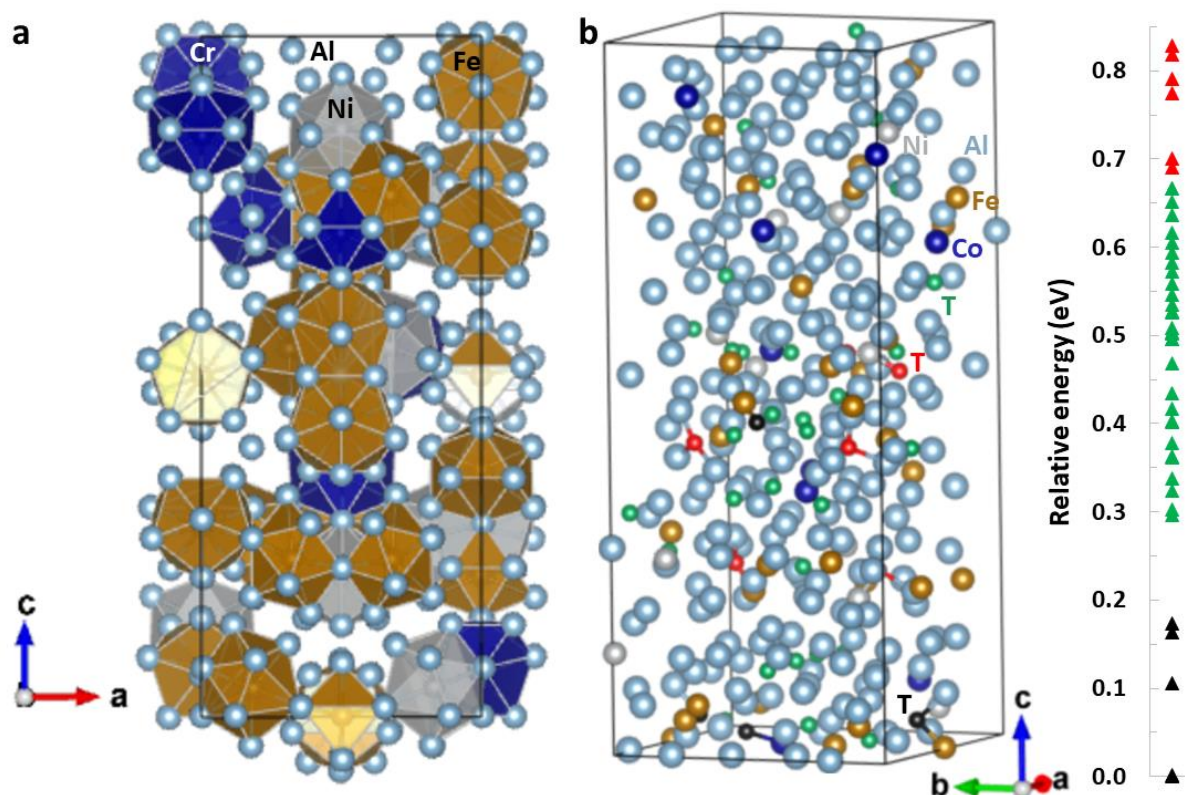
Figure 2: (a) Structural and polyhedral representation of Al$_{12}$(TM)$_{2.34}$ with 58.93 at.% Fe, 18.52 at.% Cr, and 22.54 at.% Ni per unit cell. (b) Location of the 43 interstitial tritium sites investigated in Al$_{12}$(TM)$_{2.34}$. The relative energy of each interstitial tritium site is provided in the energy diagram and the color code is reflected in the ball visual representation. Al, Fe, Co, and Ni species are represented by light blue, dark orange, dark blue, and grey spheres respectively. The interstitial tritium atoms are represented by black, green, or red spheres depending on the relative energy of their site.

For the investigation of interstitial tritium in $Al_{12}(TM)_{2.34}$, 43 interstitial sites have been explored, as shown in Figure 2b. To help localize the lowest interstitial sites in the lattice, a color code has been introduced, such that the lower energy sites, with a relative energy from 0 to 0.2 eV are represented by black spheres. Those of higher relative energy, between 0.2 and 0.7 eV have been represented by green spheres, and those with relative energy larger than 0.7 eV are represented by red spheres, as shown in Figure 2b. Interestingly, out of the four lowest energy sites, three involves tritium being bonded to Fe species and one being bonded to Cr species. Along, with previous investigations of interstitial tritium in other Al rich Fe-Al phases[6] such as $FeNiAl_5$, this suggests that interstitial tritium prefers to bind to Fe, then Cr, then Ni species.
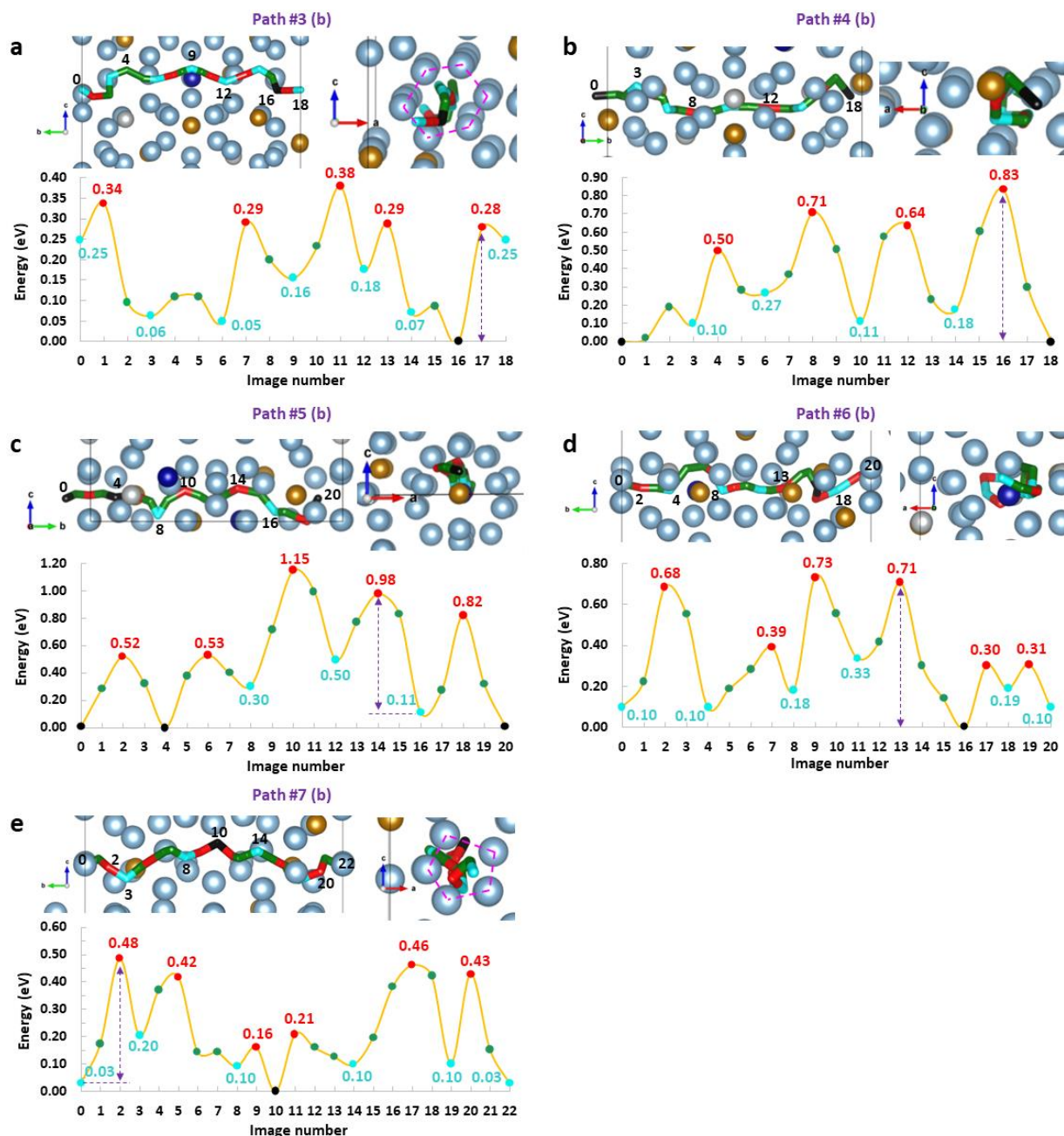
3.2 Tritium diffusion in $Al_{12}(TM)_{2.34}$

To estimate the diffusion of interstitial tritium in $Al_{12}(TM)_{2.34}$, nine diffusion pathways have been explored, among which, two are along the *a*-axis, five are along the *b*-axis, and two are along the *c*-axis. The energy diagram and visual representations of the diffusion pathways of tritium along the *a*-axis are shown in Figure 3. To facilitate the visual association between energy and position of tritium along the pathway, we have color-coded both, the dots in the energy diagram and the positions occupied by tritium along the pathway. In this color-code, the lowest energy positions have black color, local minima have cyan color, transition states or high energy positions have red color, and the energy and positions which are the transitions between low and high energy positions have green color. For each energy diagram, the largest energy barrier along the diffusion pathway is highlighted by a purple dashed vertical line. This energy barrier will be used latter on to calculate the diffusion coefficients of interstitial tritium along the pathway.
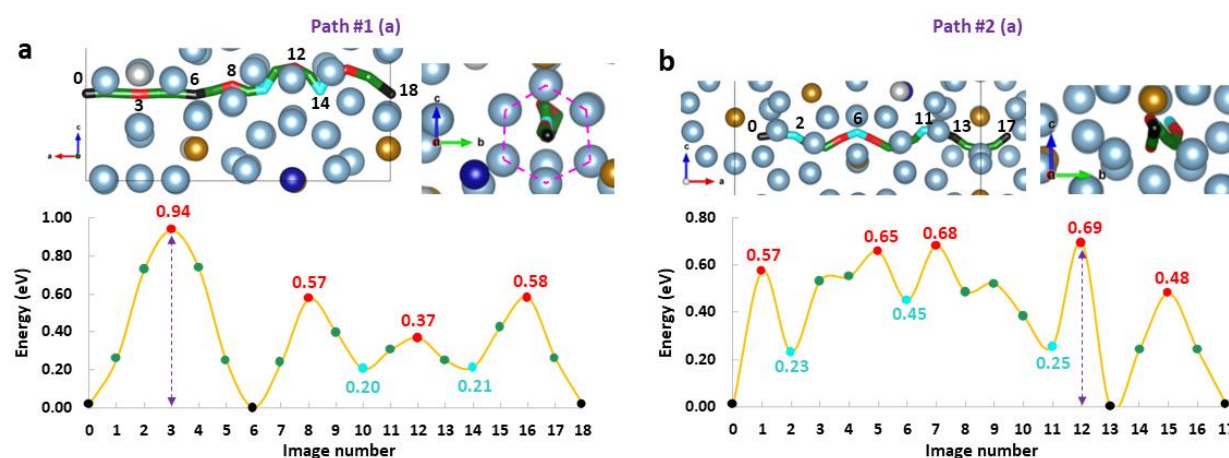
Figure 3: Energy diagrams and representation of two diffusion pathways for tritium in $Al_{12}(TM)_{2.34}$ along the *a*-axis. In the visual representations, some atoms have been removed for clarity. See main text for color coding. The largest energy barrier along each path has been highlighted by a vertical purple dashed line.

As shown in the energy diagram in Figure 3, the largest energy barrier along the two diffusion pathways investigated are 0.94 eV and 0.69 eV. Interestingly, the largest energy barrier (0.94 eV) is obtained along the pathway #1, for tritium diffusing inside a hexagonal-like column only made of Al atoms, as shown in Figure 3a. Along the pathway #2, interstitial tritium diffusing around Fe species, as shown in Figure 3b, involves an energy barrier of 0.48 eV (images #13-#17), which is the lowest energy barrier along this pathway.

For a tritium diffusion along the *b*-axis, five pathways have been investigated and are shown in Figure 4. The largest and lowest energy barrier of the series are respectively 0.87 eV, obtained along the pathway #5, and 0.28 eV, obtained along the pathway #3. In pathway #3, tritium is diffusing inside a flattened hexagonal-like column only made of Al species, as shown in Figure 4a. The second lowest energy barrier of the series, 0.45 eV, is obtained for pathway #7, in which tritium is diffusing within a pentagonal-like column made of only Al species, as shown in Figure 4e. Given the disparity of the energy barriers obtained along pathway #1 (*a*-axis) and along pathway #3 and #7 (*b*-axis), for which tritium diffuses within polygonal-like columns made of Al species only, it seems that no specific trends can be drawn about that type of structural feature as tritium diffusion in those columns can involves either the largest energy barrier (0.94 eV) or the lowest energy barrier (0.28 eV) of all the pathways investigated in this work.

Figure 4: Energy diagrams and representation of five diffusion pathways for tritium in Al$_{12}$(TM)$_{2.34}$ along the *b*-axis. In the visual representations, some atoms have been removed for clarity. See main text for color coding. The largest energy barrier along each path has been highlighted by a vertical purple dashed line.

The diffusion of tritium along the *c*-axis has been investigated for two pathways, shown in Figure 5. Given the symmetry of the Al$_{12}$(TM)$_{2.34}$ structure, those pathways spanned a half unit cell along the *c*-axis. The largest energy barrier obtained for each pathway is 0.69 eV and 0.42 eV

for pathway #8 and #9 respectively. Along these pathways, interstitial tritium is diffusing in between square-like packing of Al columns, as shown in Figure 5a and 5b.
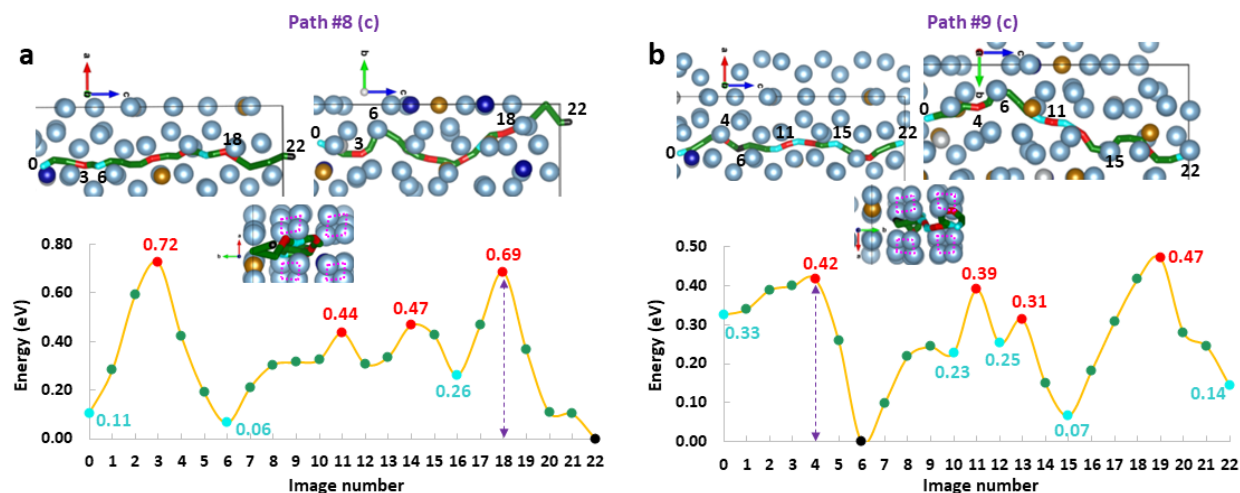

Figure 5: Energy diagrams and representation of two diffusion pathways for tritium in $Al_{12}(TM)_{2.34}$ along the *c*-axis. In the visual representations, some atoms have been removed for clarity. See main text for color coding. The largest energy barrier along each path has been highlighted by a vertical purple dashed line.

3.3   Quantifying the effect of TM mixing

To quantify the effect of mixing different transition metals in the TM sites on the energy barrier of interstitial tritium in $Al_{12}(TM)_{2.34}$, we re-calculated some diffusion pathways for tritium in $Al_{12}Fe_{2.34}$ (i.e., Fe end-member). For that, we focused on the pathways involving the lowest energy barrier for each direction along the *a*-, *b*-, and *c*-axis. Figure 6 shows the comparison of the energy landscape obtained for tritium diffusing along pathway #2, #3, and #9 in $Al_{12}Fe_{2.34}$ (black curve) and $Al_{12}(TM)_{2.34}$ (orange curve). In the case of $Al_{12}Fe_{2.34}$, as all the TM sites are occupied by the same species, the energy landscape of tritium diffusing along the pathway #2 and #3 is more symmetric than in the case where the TM sites are occupied by different transition metal species. However, Figures 6a and 6b shows that the largest energy barrier along each pathway is not very different than that obtained for $Al_{12}(TM)_{2.34}$. Indeed, the energy barrier for tritium diffusing along pathway #2 in $Al_{12}Fe_{2.34}$ is 0.59 eV, compared to 0.69 eV in $Al_{12}(TM)_{2.34}$, and 0.30 eV along pathway #3 in $Al_{12}Fe_{2.34}$, compared to 0.28 eV in $Al_{12}(TM)_{2.34}$. This suggests that these pathways are not very sensitive to species mixing in the TM sites. However, in the case of tritium diffusion along the *c*-axis, the energy barrier calculated for $Al_{12}Fe_{2.34}$ is noticeably larger than that calculated for $Al_{12}(TM)_{2.34}$, with 0.66 eV compared to 0.42 eV respectively. This is essentially due to tritium being more strongly bonded to Fe species than to Ni species. As shown by the energy diagram in Figure 2b, in which the interstitial sites with the lowest relative energy (black triangles in Figure 2b) are obtained for Fe—T and Cr—T bonds. Thus, breaking an

energetically more favorable Fe—T bond leads to a higher energy barrier than breaking a Ni—T bond.

a

b

c
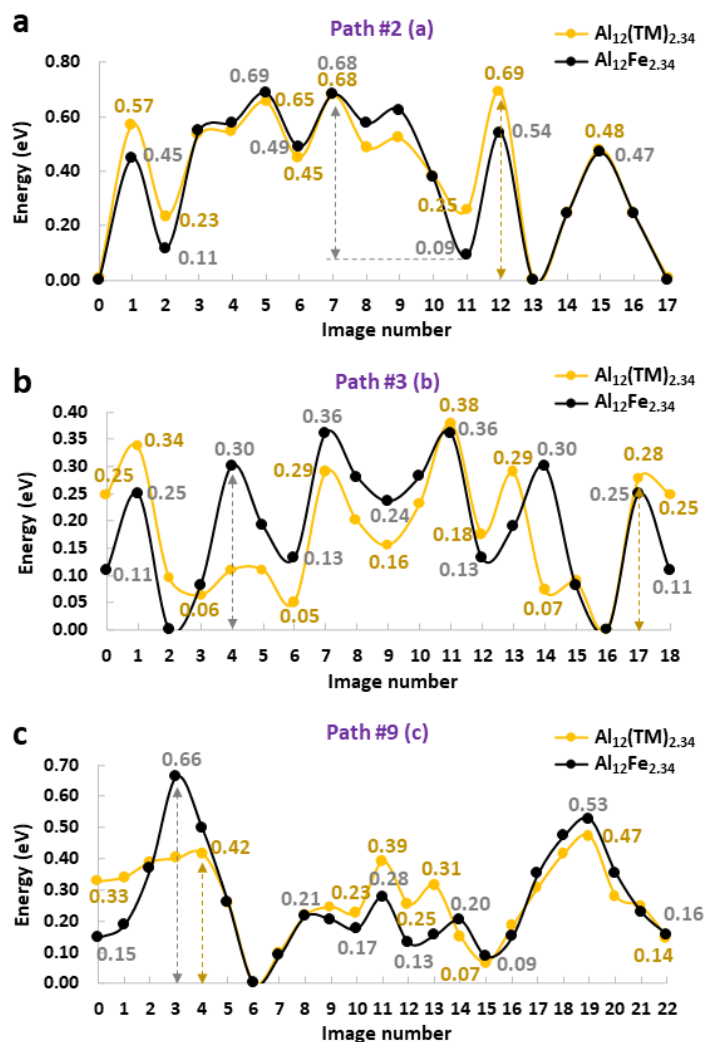
Figure 6: Comparison of the energy landscape interstitial tritium in $Al_{12}(TM)_{2.34}$ and $Al_{12}Fe_{2.34}$. The pathways are compared for the lowest diffusion pathways found along the (a) *a*-axis, (b) *b*-axis, and (c) *c*-axis. In each case, the largest energy barrier along the path has been highlighted by a vertical dashed line.

3.4   Diffusion coefficients

The diffusion coefficients of interstitial tritium, D_T , have been calculated by using the Einstein-Smoluchowski relation.[15] The diffusion coefficients can be written as:

$$D_T = \frac{d^2}{c\tau} (1)$$

where d and τ are the average distance and time between two jumps, respectively, and c is a parameter equal to 2 for one-dimensional, 4 for two-dimensional, and 6 for three-dimensional diffusion. As DFT simulations are carried out at a temperature of 0 K, in the following we will neglect the entropy of migration in the equations and approximate the Gibbs free energy of migration by the migration enthalpy, E_a. While the vibrational motions induced by elevated temperatures could induce a slight change in the diffusion coefficients calculated in this work, we note that the energy barrier is almost unaffected by temperature changes.[16]

It should be noted that equation (1) does not consider the correlation effects between interstitial atoms. This is valid in our case since we are in a dilute interstitial solid solution, where every interstitial site around the interstitial solute is empty. Therefore, the diffusion coefficient can be written as:

$$D_\mathrm{T} \approx \frac{d^2}{c} \nu_0 z e^{-\frac{E_a}{k_\mathrm{B} T}} \quad (2)$$

where z is the coordination number and ν_0 is the attempt frequency which is typically of the order of the Debye frequency, ranging from 10^{12} to 10^{13} s^{-1} for practically all solids.[15] Using statistical thermodynamics, Vineyard *et al.*[17] has shown that the jump rate, ω, which is the number of jumps per second, has an Arrhenius-type dependence on temperature and can be written as:

$$\omega = \nu_0 e^{-\frac{E_a}{k_\mathrm{B} T}} \quad (3)$$

The calculated diffusion coefficients and associated jump rates of interstitial tritium at two temperatures, 300 K and 600 K are summarized in Table 2. At 600 K, a temperature relevant to in-reactor operation, the fastest diffusion coefficient for interstitial tritium in $Al_{12}(TM)_{2.34}$ has been calculated to be 1.42×10^{-13} m^2.s^{-1}, 4.30×10^{-10} m^2.s^{-1}, and 2.30×10^{-10} m^2.s^{-1} along the *a*-, *b*-, and *c*-axis respectively. In the case of $Al_{12}Fe_{2.34}$, the diffusion coefficients are 5.47×10^{-12} m^2.s^{-1}, 1.10×10^{-9} m^2.s^{-1}, and 1.63×10^{-12} m^2.s^{-1} along the *a*-, *b*-, and *c*-axis respectively. For both materials, the fastest diffusion coefficient is obtained along the *b*-axis and it is in the order of 10^{-10} m^2.s^{-1} and 10^{-9} m^2.s^{-1} for $Al_{12}(TM)_{2.34}$ and $Al_{12}Fe_{2.34}$ respectively. Compared to previously calculated[6] diffusion coefficients for interstitial tritium in Al-rich phases, such as Fe_2Al_x, Fe_4Al_{13}, and $FeNiAl_5$ for which $D_\mathrm{T} \leq 10^{-11}$ m^2.s^{-1}, $\approx 10^{-12}$ m^2.s^{-1}, and $D_\mathrm{T} \approx 10^{-13}$ m^2.s^{-1}, tritium diffusion is the fastest in $Al_{12}(TM)_{2.34}$, with a diffusion coefficient for near surface $Al_{12}(TM)_{2.34}$ of $\approx 10^{-10}$ m^2.s^{-1}.

Material	Pathway	d (Å)	E_a (eV)	T=300 K		T=600 K	
				D_T (m².s⁻¹)	ω (jump/s)	D_T (m².s⁻¹)	ω (jump/s)
	Path_1 (a)	4.42	0.94	1.05×10^{-22}	0	8.28×10^{-15}	127,159
	Path_2 (a)	1.63	0.69	2.27×10^{-19}	26	1.42×10^{-13}	16,004,978
$Al_{12}(TM)_{2.34}$	Path_3 (b)	1.70	0.28	1.91×10^{-12}	197,791,228	4.30×10^{-10}	$>4.45 \times 10^{10}$
	Path_4 (b)	3.82	0.83	5.55×10^{-21}	0	5.20×10^{-14}	1,067,350

	Path_5 (b)	4.12	0.87	1.37×10^{-21}	0	2.78×10^{-14}	492,404
	Path_6 (b)	4.01	0.71	6.32×10^{-19}	12	5.81×10^{-13}	10,870,824
	Path_7 (b)	2.77	0.45	7.04×10^{-15}	275,634	4.24×10^{-11}	$>1.66\times10^{9}$
	Path_8 (c)	6.70	0.69	3.83×10^{-18}	26	2.39×10^{-12}	16,004,978
	Path_9 (c)	4.83	0.42	6.83×10^{-14}	879,651	2.30×10^{-10}	$>2.97\times10^{9}$
	Path_2 (a)	3.85	0.59	6.06×10^{-17}	1,226	5.47×10^{-12}	110,717,971
$Al_{12}Fe_{2.34}$	Path_3 (b)	3.30	0.30	3.32×10^{-12}	91,247,677	1.10×10^{-9}	$>3.02\times10^{10}$
	Path_9 (c)	4.14	0.66	4.67×10^{-18}	82	1.63×10^{-12}	28,591,965

Table 2: Summary of the average distances and energy barriers obtained for each pathway investigated. The diffusion coefficients and jump rates for interstitial tritium diffusion in $Al_{12}(TM)_{2.34}$ and $Al_{12}Fe_{2.34}$ have been calculated for T=300 K and 600 K. The calculations used the following parameter values: k_B=8.6173×10^{-5} eV.K^{-1}, ν_0=10^{13} s^{-1}, c=6, and z= 2.

3.5   Interstitial tritium in Al₂O

The insertion of interstitial tritium in Al_2O followed by atomic optimization yielded a strong disordering of the structure, as shown in Figure 7. This is resulting from oxygen species being very reactive to form O—T bonds with the interstitial tritium added in the lattice. The formation of such bond induced a complete reorganization of the bonding pattern between Al and O species leading to a strongly disordered structure. Given the large modifications in the structure of Al_2O, we did not continue the investigation of tritium diffusion pathways as the end-structure is not relevant to the initial structure, as observed by TEM imaging. While the disordering of Al_2O is not seen in the experimental TEM images, two possible effects could be in play: (*i*) experimentally, Al_2O is observed as a transition between surface Al_2O_3 and near surface $Al_{12}(TM)_{2.34}$ phases thus it could be possible that those two phases are stabilizing Al_2O. (*ii*) While the bonding pattern in defect-free bulk Al_2O is very impacted by the insertion of interstitial tritium, the potential presence of Al vacancies in Al_2O could readily accommodate the formation of O—T bonds with less structural distortions. However, it is currently unknown how Al_2O would accommodate Al vacancies and how those would affect the Al—O bonding pattern. Additional numerical simulations should be performed to investigate the stability of Al_2O with respect to defect creation.
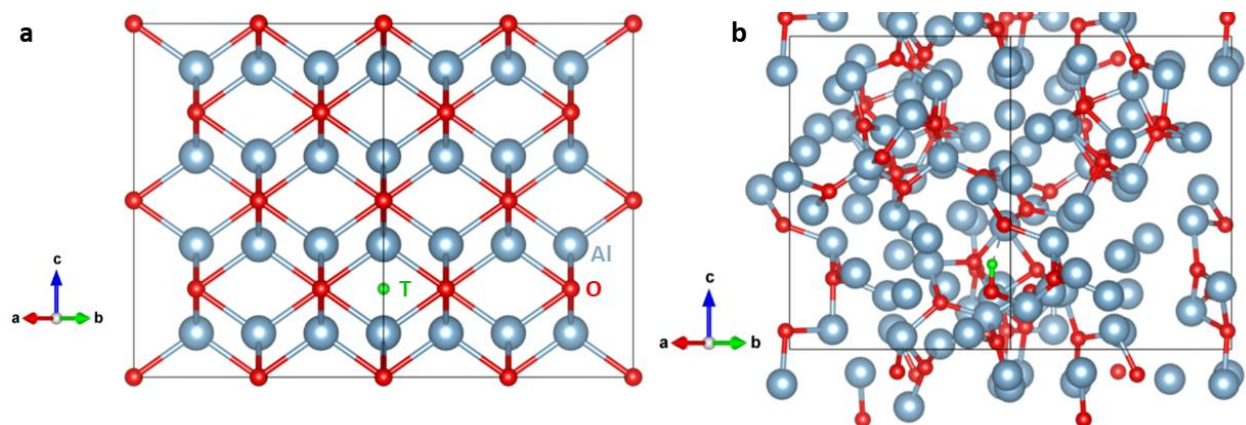
Figure 7: Visual representation of interstitial tritium in Al₂O (a) before and (b) after atomic optimization.

Conclusion

Density functional theory simulations have been carried out to investigate the diffusion of interstitial tritium in $Al_{12}(TM)_{2.34}$ and Al_2O bulk phases. While the insertion of interstitial tritium in Al_2O lead to a strong disordering of the structure, we only investigated interstitial tritium in $Al_{12}(TM)_{2.34}$ and its iron end-member (i.e., $Al_{12}Fe_{2.34}$). Nine diffusion pathways have been investigated along the *a*-, *b*-, and *c*-axis of $Al_{12}(TM)_{2.34}$. The direction of fastest diffusion for interstitial tritium is found to be along the *b*-axis, with a calculated diffusion coefficient of $\approx 10^{-10}$ $m^2.s^{-1}$ at 600 K, which is faster than those previously calculated for interstitial tritium in other Al-rich phases such as Fe_2Al_x, Fe_4Al_{13}, and $FeNiAl_5$. The comparison of the energy landscape between $Al_{12}(TM)_{2.34}$ and $Al_{12}Fe_{2.34}$ for the fastest diffusion pathways in each axis direction, found that some pathways are not sensitive to transition metal mixing, while other are more affected, leading to higher energy barrier in $Al_{12}Fe_{2.34}$ in part due to a more energetically favorable formation of Fe—T bond compared to Ni—T. However, we found that both materials have similar diffusion coefficients as the fastest diffusion pathways occurs along pathways that are not very sensitive to transition metal mixing.

Acknowledgments

4.0   References

1.   Senor, D.J. "Science and technology in support of the tritium modernization program". *Report PNNL-31479*, Pacific Northwest National Laboratory **(June 2021)**.

2.   United States Government Accountability Office (GAO) "National Nuclear Security Administration Needs to Ensure Continued Availability of Tritium for the Weapons Stockpile". *Report GAO-11-100 Nuclear Weapons* **(October 2010)**.

3.   Bums, K.A.; Love, E.F.; Thomhill, C.K. "Description of the tritium-producing burnable absorber for the commercial light water reactor". *PNNL-22086 Rev. 19*, TTQP-1-015, Pacific Northwest National Laboratory **(February 2012)**.

4.   Jiang, W. et al. "Carbonaceous deposits on aluminide coatings in tritium-producing assemblies". *Nuclear Materials and Energy* **25**, 100797 (2020).

5.   Olszta, M. "Advanced Electron Microscopy for the TTP Program". Presentation **(May 2022)**.

6.   Sassi, M.; Senor, D.J. "Tritium diffusion in Fe-Al aluminide coating bulk phases". Report PNNL-32040 **(September 2021)**.

7.   Kresse, G.; Furthmüller, J. "Efficient iterative schemes for ab initio total-energy calculations using a plane-wave basis set". *Phys. Rev. B* **54**, 11169-11186 (1996).

8.   Perdew, J.P.; Burke, K.; Ernzerhof, M. "Generalized Gradient Approximation Made Simple". *Phys. Rev. Lett.* **77**, 3865-3868 (1996).

9.   Sui, H. X.; Liao, X. Z.; Kuo, K. H.; Zou, X.; Hovmöller, S. Structural Model of the Orthorhombic Non-Fibonacci Approximant in the $Al_{12}Fe_2Cr$ Alloy. *Acta Cryst.* **B53**, 587-595 (1997).

10.   Hoch, M.; Johnston, H.L. Formation, Stability and Crystal Structure of the Solid Aluminium Suboxides. Al_2O and AlO. *J. Am. Chem. Soc.* **76**, 2560-2561 (1954).

11.   Monkhorst, H.J.; Pack, J.D. Special points for Brillouin-zone integrations. *Phys. Rev. B* **13**, 5188 (1976).

12.   Sheppard, D.; Terrell, R.; Henkelman, G. Optimization methods for finding minimum energy paths. *J. Chem. Phys.* **128**, 134106 (2008).

13.   Sheppard, D.; Xiao, P.; Chemelewski, W.; Johnson, D.D.; Henkelman, G. A generalized solid-state nudged elastic band method. *J. Chem. Phys.* **136**, 074103 (2012).

14.   Okhotnikov, K.; Charpentier, T.; Cadars, S. Supercell program: a combinatorial structure-generation approach for the local-level modeling of atomic substitutions and partial occupancies in crystals. *J Cheminform* **8**, 17 (2016).

15.   Mehrer, H. Diffusion in solids: Fundamentals, methods, materials, diffusion-controlled processes. *Springer Series in Solid State Science*. 155 (2007).

16.   Mantina, M.; Wang, Y.; Arroyave, R.; Chen, L.Q.; Liu, Z.K.; Wolverton, C. First-principles calculations of self-diffusion coefficients. *Phys. Rev. Lett.* **100**, 215901 (2008).

17. Vineyard, G.H. Frequency factors and isotropy effects in solid state rate processes. *J. Phys. Chem. Solids* **3**, 121-127 (1957).

Pacific Northwest
National Laboratory

902 Battelle Boulevard
P.O. Box 999
Richland, WA 99354
1-888-375-PNNL (7665)

www.pnnl.gov